Analysis of a Prototype Multi-Detector Fast-Neutron Radiography Panel

Christian X. Young[1*], Chloe A. Browning[2], Ryan J. Thurber[2], Matthew R. Smalley[3], Michael J. Liesenfelt[2], Jason P. Hayward[2], Nicole McFarlane[3], Michael P. Cooper[1] and Jeff R. Preston[1]

[1*]Y-12 National Security Complex, 301 Bear Creek Rd., Oak Ridge, 37830, Tennessee, USA.
[2]Department of Nuclear Engineering, University of Tennessee, 863 Neyland Dr., Knoxville, 37916, Tennessee, USA.
[3]Min H. Kao Department of Electrical Engineering and Computer Science, University of Tennessee, 1520 Middle Dr., Knoxville, 37996, Tennessee, USA.

*Corresponding author(s). E-mail(s): christian.young@pxy12.doe.gov;
Contributing authors: cbrowni5@vols.utk.edu ; rthurber@vols.utk.edu ; msmalle2@vols.utk.edu ; mliesenf@utk.edu; jhayward@utk.edu; mcf@utk.edu; Michael.Cooper@pxy12.doe.gov; Jeffrey.Preston@pxy12.doe.gov;

Abstract

A multi-detector fast neutron radiography panel was built using the previous work on scalable neutron radiography using the IDEAS ROSSPAD readout module. A new aluminum housing was built to accommodate a large number of detectors tiled together. Additional changes to startup and processing code were made to operate the detector as one cohesive unit. Spatial resolution of the full panel using Cs-137 gammas was reported to be 0.42 line pairs per centimeter at 90% MTF and 2.09 line pairs per centimeter at 10% MTF. Three neutron radiographs generated using a Cf-252 fission neutron source were used to determine the spatial resolution of the panel for neutrons. The experiments had 90% MTF values of 0.24, 0.3, and 0.27 line pairs per

centimeter and 10% MTF values of 1.30, 1.46, and 1.40 line pairs per centimeter. An example neutron radiograph was also used to prove that the radiography panel can perform true neutron radiography.

Keywords: Fast Neutron Radiography, Proton Recoil Neutron Radiography, Neutron Counting, Neutron Radiography, Radiation Imaging, Silicon Photonics

1 Introduction

The growth of neutron radiography has led to many innovative concepts and designs for both the neutron generator and the neutron detection system. Neutron imaging systems, particularly using fast (14.1 MeV) neutrons, offer a wide range of detection methods to generate images, including camera-and-mirror setups [1][2][3], thin-screen converter panels [4], and photomultiplier (PMT) arrays [5][6]. All of these systems have advantages and disadvantages given the application space they are applied to. All of these systems, however, are limited in their scalability and portability. Prior work by this group demonstrated a new imaging concept comprised of commercial-off-the-self detectors [7]. These detectors, the IDEAS ROSSPAD, use a board containing an array of 64 SensL MICROFJ-60035-TSV Silicon Photomultipliers (SiPMs) and can be easily tiled together into a larger radiography panel [8]. This new form factor provided an alternative to the systems currently in use that more easily fit the scope of the use case it was built for.

For generating radiography images, the IDEAS ROSSPAD readout module showed promising results using a weighted-average localization method. Images generated using both Cs-137 and Cf-252 achieved sub-SiPM spatial resolution. Cs-137 images have a 10% modulation transfer function (MTF) resolution of 2.32 line pairs per centimeter and Cf-252 images have a 10% MTF resolution of 3.35 line pairs per centimeter [7]. For a bare board containing 6-mm-pitch SiPMs, the theoretical spatial resolution is 0.833 line pairs per centimeter. This method of generating images is also simple to implement and compute, decreasing image generation times.

Single-ROSSPAD imaging is incredibly useful for a wide range of applications. The size of these detectors, however, limits their use as a standalone imaging system. A single ROSSPAD is limited to a detection area of 50 mm by 50 mm [8]. Smaller commercially-available x-ray imaging panels easily exceed the size of a single ROSSPAD. For example, the Varex 1207 CMOS Flat Panel Detector, their smallest area imaging system, has an active area of 120 mm by 70 mm, over three times larger than a single ROSSPAD [9]. Current state-of-the-art neutron imaging systems found in laboratory settings also have larger active areas. A single detector package used in the Advanced Portable Neutron Imaging System (APNIS) at Oak Ridge National Laboratory used segmented

scintillator blocks that measured 104 mm by 104 mm, though the spatial resolution was limited to 1 centimeter [5]. These blocks could be tiled together using detector electronics used in medical imaging to build a larger radiography panel [5]. Bishnoi et al. had a larger active area than the ROSSPAD, 300 mm by 300 mm, while maintaining millimeter-scale spatial resolution [2].

This research expands on the original ROSSPAD imaging system, using multiple ROSSPAD detectors tiled together to make one larger radiography panel. While the original ROSSPAD processing routines used in Young et al. were designed to be used in a scalable radiography panel, some changes were needed in order to produce high-quality images from detector data [7]. Spatial resolution and image processing will be compared between the two systems to demonstrate the feasibility of building large imaging arrays from multiple detectors sharing the same set of data. An example large-scale radiograph will be included to showcase the capabilities of this system.

2 Methods

2.1 Detector Hardware

A large-scale radiography panel built with the ROSSPAD readout module utilized the same detector hardware as the original work done by this group [7]. The larger radiography panel still uses a 3-mm-thick sheet of EJ-200 plastic scintillator coupled with a 3-mm-thick sheet of polycarbonate as a light spreader. This scintillator package, however, is much larger, measuring 300 mm by 300 mm instead of 50 mm by 50 mm. This larger scintillator package can now cover a 6 by 6 area of ROSSPAD detectors. By using one continuous package, light from a single event can spread to multiple ROSSPADs if the event occurs at the edge or corner of a detector. This will enable cross-ROSSPAD localization, reducing the issues of events not spreading to the true edge of the detector as shown in the single-ROSSPAD work.

A new aluminum housing was designed to accommodate the array of detectors. A solid aluminum lid keeps the scinitllator package and SiPMs contained and protected. A gasket material is placed between the SiPM board and the rest of the ROSSPAD module to keep the area under the lid light tight. Putting all of the ROSSPADs together in one place generated enough heat to require active cooling. A total of twelve (six inlet and six outlet) Noctua NF-A4x20 fans actively cooled the ROSSPAD detectors [10]. Removable handles and a removable base plate allow for easy transport and deployment of the detector. Figure 1 shows the front of the panel with the aluminum lid attached. Figure 2 shows the inside of the panel before ROSSPADs were added.

Initial testing of the multi-ROSSPAD panel was performed using a 4 by 3 area of detector modules. Time constraints and limited computer hardware capability limited the ability to evaluate a full 6 by 6 radiography panel. It should be noted that methods employed on the smaller 4 by 3 area will still scale to any size, even beyond the originally planned 6 by 6 panel.

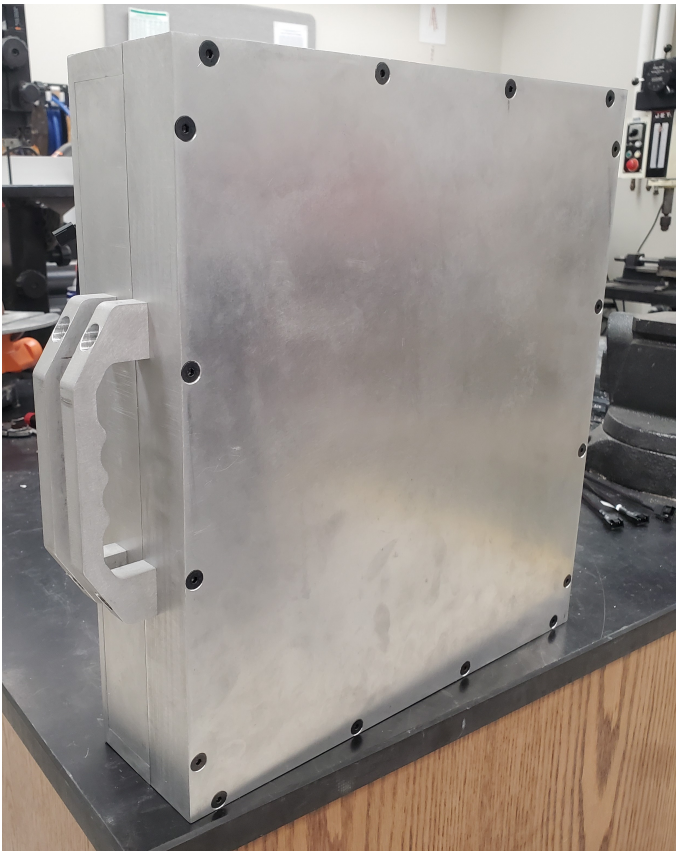

Fig. 1: The front of the full-panel neutron radiography system designed around the ROSSPAD module.

2.2 Data Handling and Processing

Data handling and processing saw minimal changes between the single and multi-ROSSPAD systems. Data collection was already performed through a Power-over-Ethernet (PoE) switch, which could handle all of the ROSSPADs added to the full panel. Loops were added to allow for parallel ROSSPAD startup across the whole panel, decreasing detector startup time. Background and noise correction was exactly the same, but gain correction was scaled to determine the optimal gain setting using the average gain value on all of the SiPMs across all of the ROSSPADs in the panel instead of the SiPMs on just one individual ROSSPAD. This means that the response from any SiPM will be the same for the same amount of light collected regardless of where it occurred in the panel.

All but one ROSSPAD internal setting was kept to the default, much like the singular ROSSPAD work. The default triggering threshold of 28 units was not enough to allow for cross-ROSSPAD localization. Figure 3 shows that with

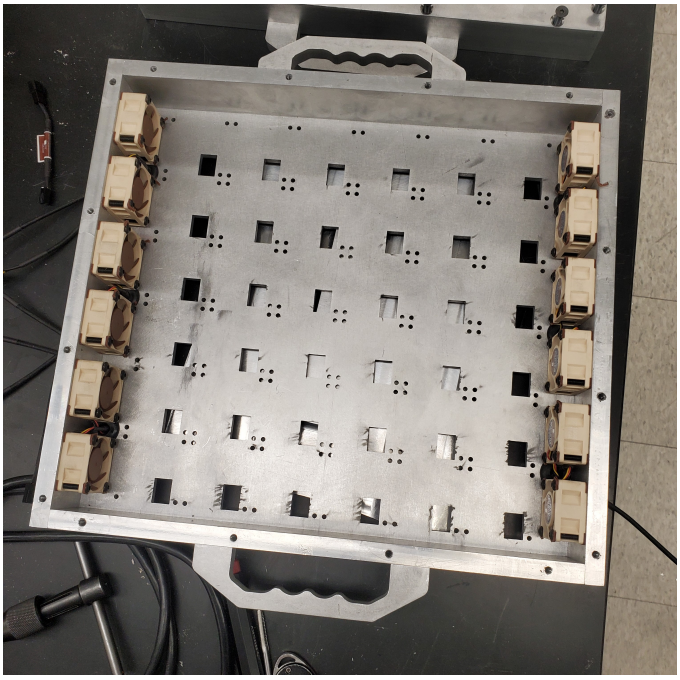

Fig. 2: Interior of the full-panel neutron radiography system before the installation of ROSSPAD modules.

the triggering threshold set to 28 units, a typical radiation event that occurs at the edge of a detector does not produce enough light to set multiple detectors off. This limits the ability to perform cross-ROSSPAD localization, artifacts that occur at the boundaries where ROSSPADs meet. Figure 4 shows the result of lowering the triggering threshold to 20 units. Now when an event occurs at the edge of a ROSSPAD, the neighboring ROSSPAD is set off as well. The event can then be localized using the data from both detectors. Lowering the threshold does increase the amount of noise in the system, but post-processing techniques will reduce the impact of noise in the final images.

2.3 Image Generation

A new step in the image generation processes had to be added to the previous process used in Reference [7]. Figure 5 shows a flood field taken with the 4 by 3 area of ROSSPADs. Due to changes in the detector package, a large amount of artifacts show up within the image. To compensate for this, a method was borrowed from traditional x-ray radiography that uses flood fields at various beam intensity levels to correct the response of the pixels and make the image appear even [11].

The radiography panel works in a particle-counting mode as opposed to integral mode commonly used by traditional x-ray radiography panels. This

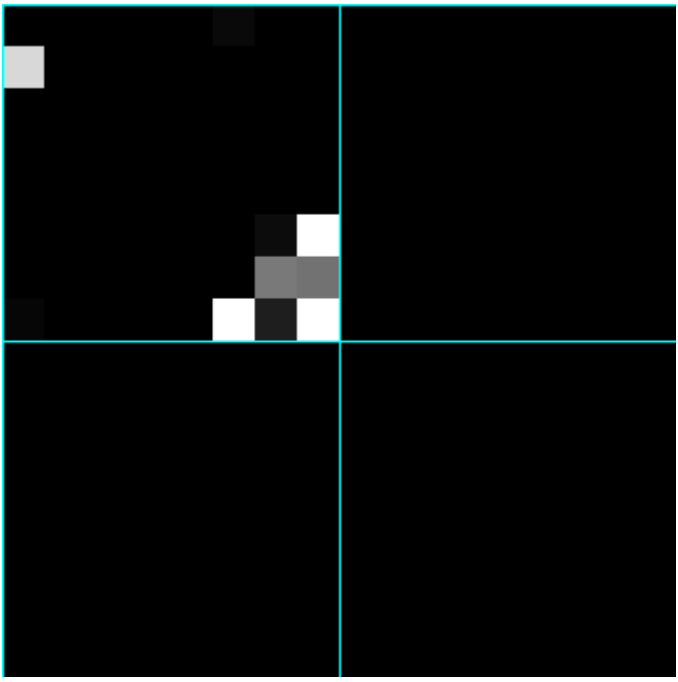

Fig. 3: A single-event trigger map with the higher triggering threshold value (28) set. The event space is shown across four ROSSPADs (cyan grid lines).

means that the lowest flood field level can be assumed to be a value of zero in every pixel. The radiography panel response is assumed to be linear so that the flood field correction formula can be simplified to:

$$P_{(x,y)} = \frac{R_{(x,y)}}{F_{(x,y)}} \tag{1}$$

where $P_{(x,y)}$ is the value of the (x, y) pixel in the post-correction image, $R_{(x,y)}$ is the value of the (x, y) pixel in the raw, uncorrected image, and $F_{(x,y)}$ is the value of the (x, y) pixel in a flood field using the same source of radiation. Equation 1 can be applied to any image with ImageJ, allowing for the process of artifact correction to be done [12]. Corrected flood fields are provided in the Results section of this paper.

One experiment was performed using a Cs-137 gamma source producing a collimated line across the face of the detector. Figure 6 shows two stacks of 3.8 ± 0.1 cm thick tungsten blocks (equivalent to approximately 7 mean free paths for a 662 keV gamma ray [13]) placed on top of each other, with a 0.2 ± 0.003 cm thick gap separating to two stacks apart. The radiography panel was placed at a 10° angle so that the line can fall over multiple ROSSPAD boundaries in both x and y, and the 0.105 mCi Cs-137 gamma source was placed approximately 25.4 ± 0.1 cm away from the faces of the tungsten blocks.

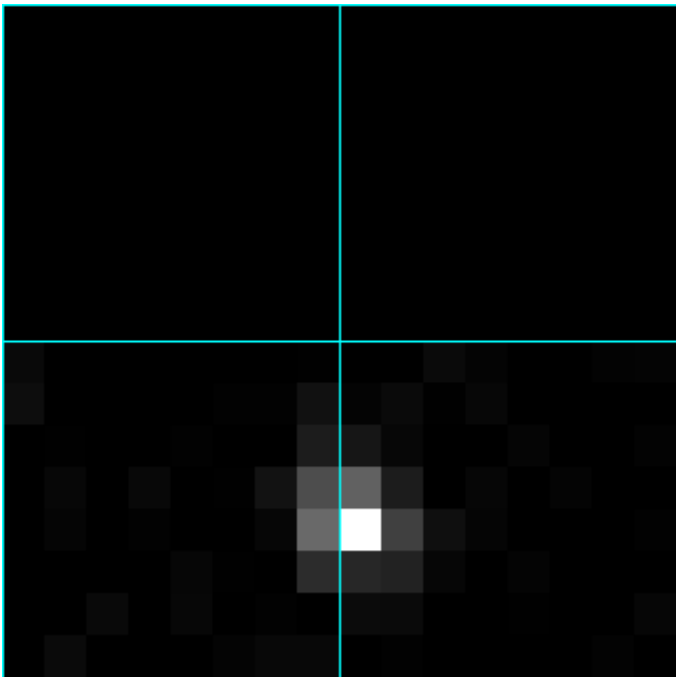

Fig. 4: A single-event trigger map with the lower triggering threshold value (20) set. The event space is shown across four ROSSPADs (cyan grid lines).

Three experiments were performed using a Cf-252 spontaneous fission neutron source. The first experiment, shown in Figure 7, used a collimated edge comprised of high-density polyethylene (HDPE) measuring 15.3 ± 0.1 cm thick (equivalent to approximately 5 mean free paths assuming an average fission neutron energy of 2.105 MeV [14]), placed at the face of the panel. The radiography panel was again placed at a 10° angle. The 0.090 mCi Cf-252 neutron source was placed approximately 14.0 ± 0.1 cm away from the face of the HDPE blocks. The source was placed on a lead shelf-like object that allowed for approximately 2.5 ± 0.1 cm of lead to shield the detector from the gamma rays coming off of the daughter products of the source.

The second Cf-252 experiment, shown in Figure 8, was performed in an attempt to reduce the geometric unsharpness created by the setup and potentially improve spatial resolution. Instead of an edge, a collimated line was generated using two 5.1 ± 0.1 cm HDPE blocks placed 0.2 ± 0.003 cm apart, similar to the experiment performed with the Cs-137 gamma source. The source configuration was kept unchanged between this and the last setup, with the 0.090 mCi Cf-252 neutron source placed approximately 14.0 ± 0.1 cm away from the face of the HDPE blocks. The same lead object that allowed for approximately 2.5 ± 0.1 cm of lead to shield gamma rays from the Cf-252 source.

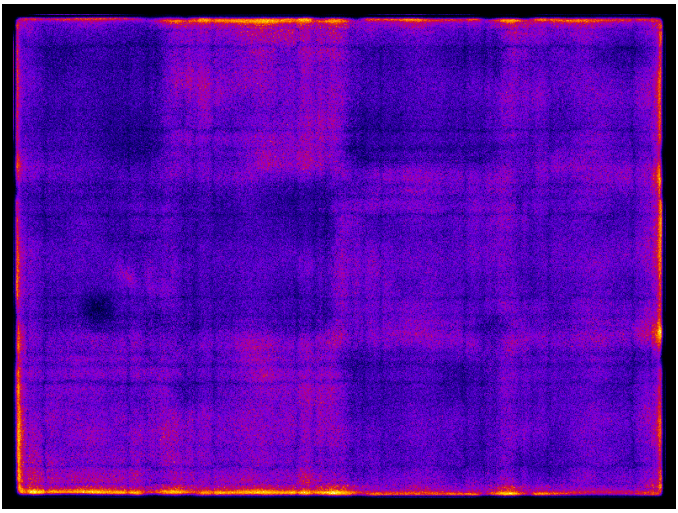

Fig. 5: Full-panel flood fields using a Cf-252 neutron source weighted by the total signal from events in pixel. ($N = 1.17 \times 10^7$ counts)

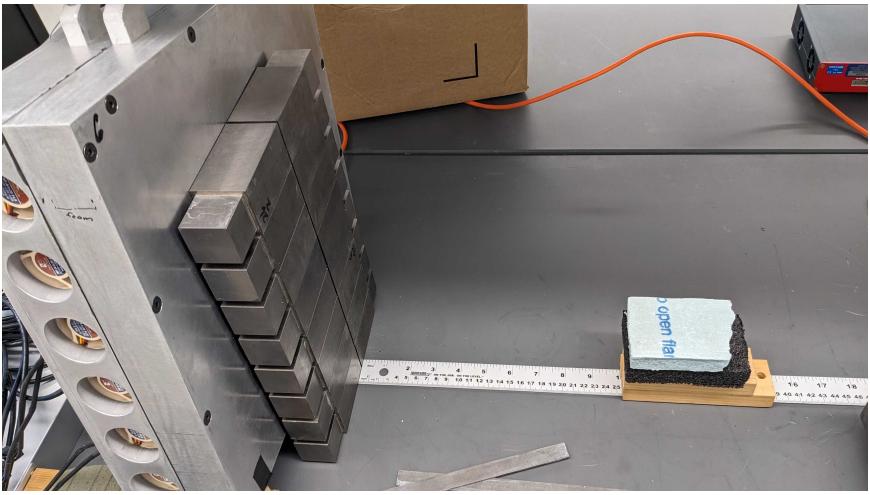

Fig. 6: Experimental setup for generating a collimated Cs-137 line image on the full radiography panel.

The third Cf-252 experiment was taken to make the most direct comparison to the spatial resolution found in Young et al. by mimicing the previous experimental setup as closely as possible [7]. Figure 9 shows a stack of high-density polyethylene (HDPE) measuring 15.3 ± 0.1 cm thick (equivalent to approximately 5 mean free paths assuming an average fission neutron energy of 2.105 MeV [14]) placed approximately 22.9 ± 0.1 cm from the face of the

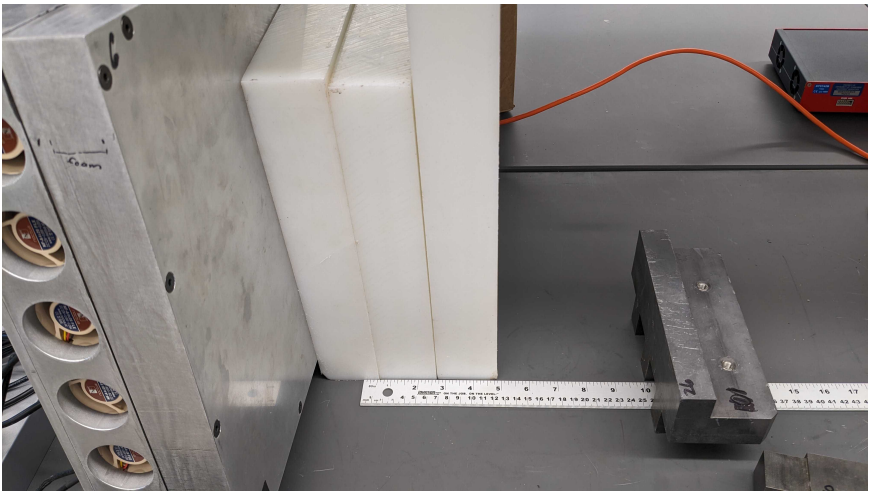

Fig. 7: First experimental setup for generating a collimated Cf-252 image.

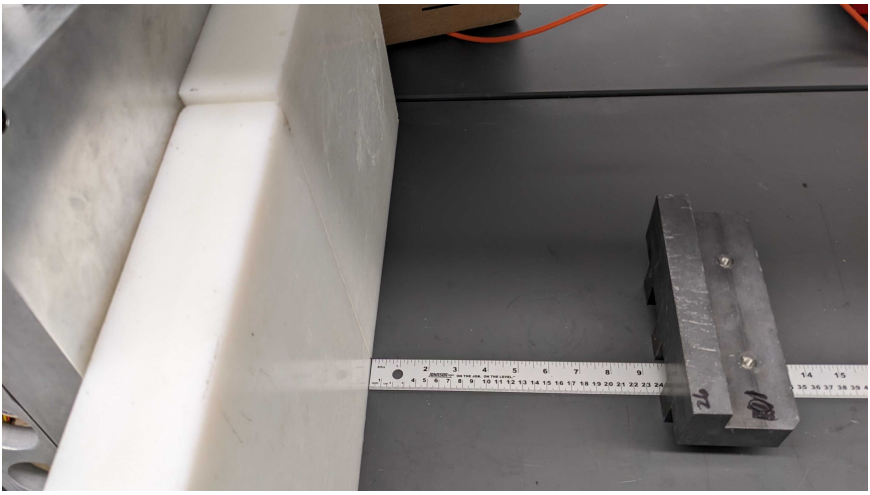

Fig. 8: Second experimental setup for generating a collimated Cf-252 image.

panel. Because EJ-200 puts out approximately 10,000 scintillation photons per MeV of energy transferred from a neutron, slowing the neutrons down using HDPE will lower the light output from any neutrons that are scattered in the HDPE and still interact in the EJ-200 scintillator.[15] At a certain threshold, low-energy events will not produce enough light to be recorded by the ROSS-PAD modules. A 0.090 mCi Cf-252 neutron source was placed approximately 40.6±0.1 cm away from the face of the HDPE blocks. A sheet of lead 0.2±0.003 cm thick was placed in front of the Cf-252 source to block out some of the gamma rays.

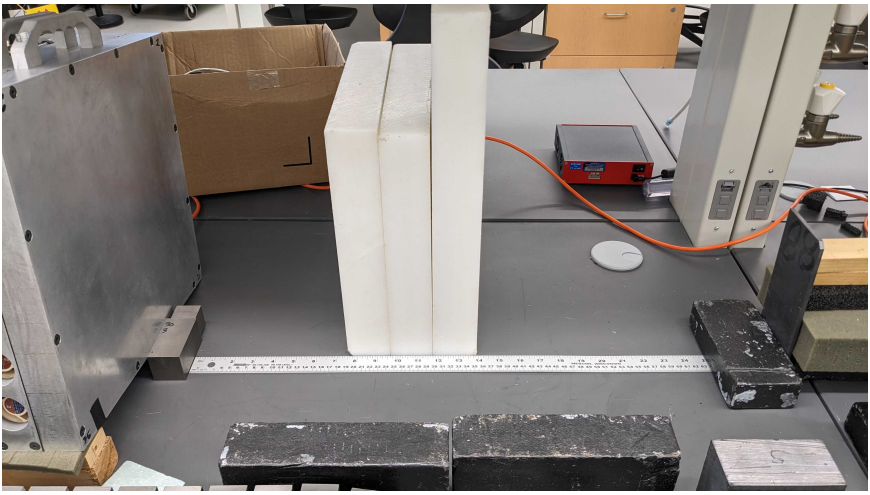

Fig. 9: Third experimental setup for generating a collimated Cf-252 image.

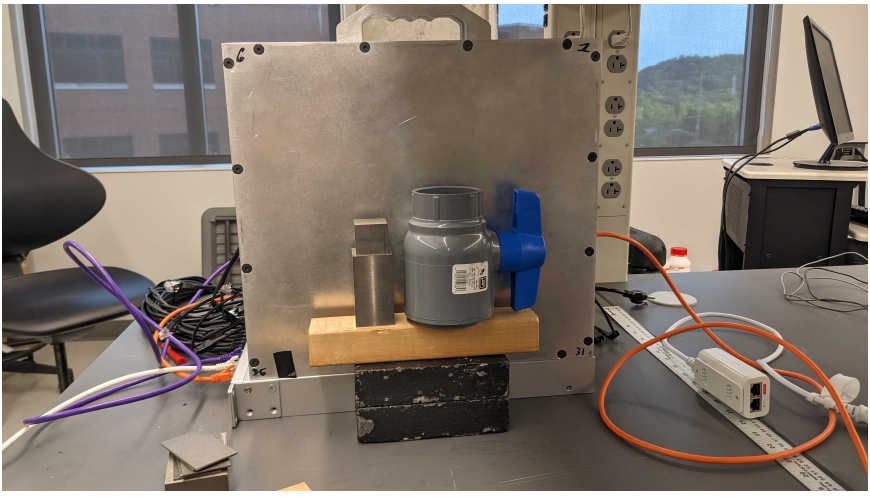

Fig. 10: A tungsten block and a plastic pipe valve in front of the radiography panel.

A demonstration image was also taken to showcase the capabilities of this system. Figure 10 shows a simple test using a 3.81 ± 0.1 cm thick tungsten block with a small, reduced size portion on top and a plastic ball valve, which were irradiated using neutrons from the 0.090 mCi Cf-252 neutron source.

3 Results

3.1 Cesium-137 Images

Figure 11 shows the uncorrected and corrected count-weighted line images. While the line still appears to have some artifacting present, particularly in areas where dual-ROSSPAD imaging is needed to localize near the edges of two detectors, the line still appears straight and well collimated, much like the results from the single-ROSSPAD imaging. The line was rotated 10° in ImageJ, and an average profile of the line was generated and exported to Excel. Both the averaged line values from ImageJ and a fitted Gaussian curve to the values are shown in Figure 12. On the full panel, the Gaussian fit appeared to fit the profile from ImageJ better than the fit on the single ROSSPAD, though there is still some deviation on the left side of the profile. Figure 13 shows a 90% spatial resolution of approximately 0.42 line pairs per centimeter and a 10% spatial resolution of approximately 2.09 line pairs per centimeter. Note that the line connecting the data points are for performing conservative linear interpolation in order to determine the 90% and 10% MTF values. Both of these values are slightly less than the same values for the Cs-137 MTF in Young et al. [7]. This may be the result of geometric unsharpness [16]. The gap between the face of the scintillator and the tungsten blocks for the single ROSSPAD was only the width of a few pieces of tape, where the larger radiography panel has several millimeters of foam and aluminum separating the tungsten blocks and the scintillator package.

3.2 Californium-252 Images

Figure 14 shows the uncorrected and corrected signal-weighted edge images for the first experiment. The edge in the uncorrected image is almost impossible to see, but the corrected image does make the edge significantly more clear, highlighting the importance of correcting the radiographs using a flood field. Some slight artifacting at the boundaries of ROSSPADs can still be seen in the corrected image; overall, the radiograph is clear enough to use for an MTF measurement. The edge was rotated 10° in ImageJ, and an average profile of the line was generated. Both the averaged line values from ImageJ and a fitted ERF function to the values are shown in Figure 15. Since significantly more counts were used to generate this profile compared to the profile on the single ROSSPAD in Reference [7], there is significantly less variation, allowing for the functional fit to approximate the experimental data much more closely. Figure 16 shows a 90% spatial resolution of approximately 0.24 line pairs per centimeter and a 10% spatial resolution of approximately 1.30 line pairs per centimeter. Both of these values are significantly less than the same values for the Cf-252 MTF in Young et al. [7]. While some loss of spatial resolution was expected due to the geometric unsharpness added from the design of the radiography panel, the amount of resolution lost does not correlate to the spatial resolution change seen in the Cs-137 MTF.

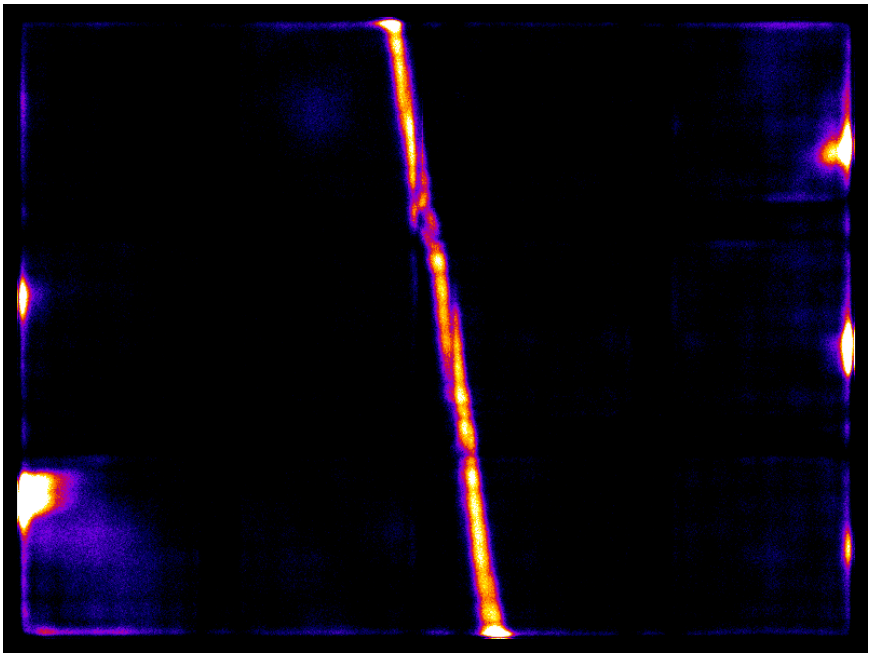

(a) Uncorrected

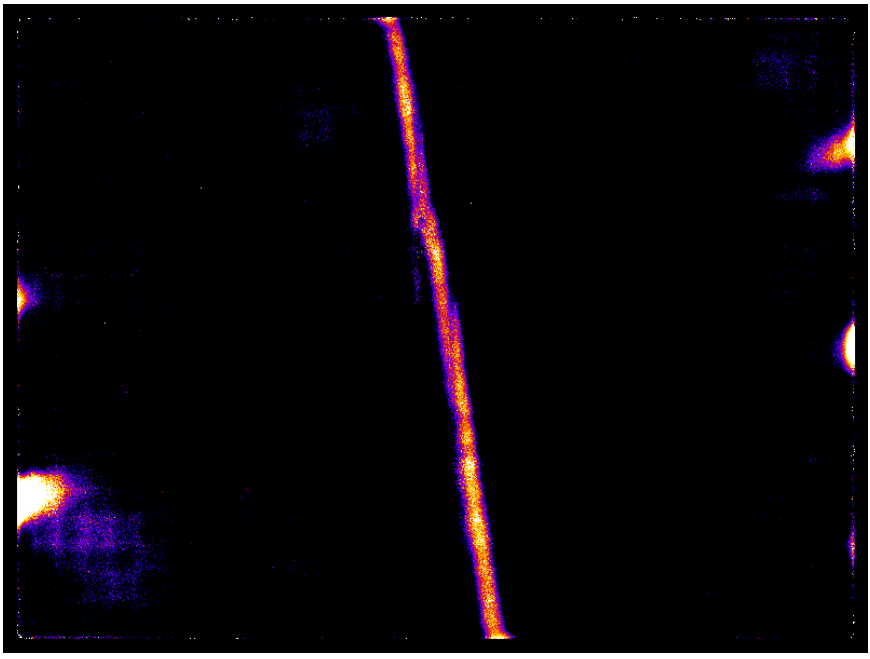

(b) Corrected

Fig. 11: Full-panel Cs-137 collimated line images that are a) before flood field correction and b) after flood field correction. (N = 7.63×10^6 counts)

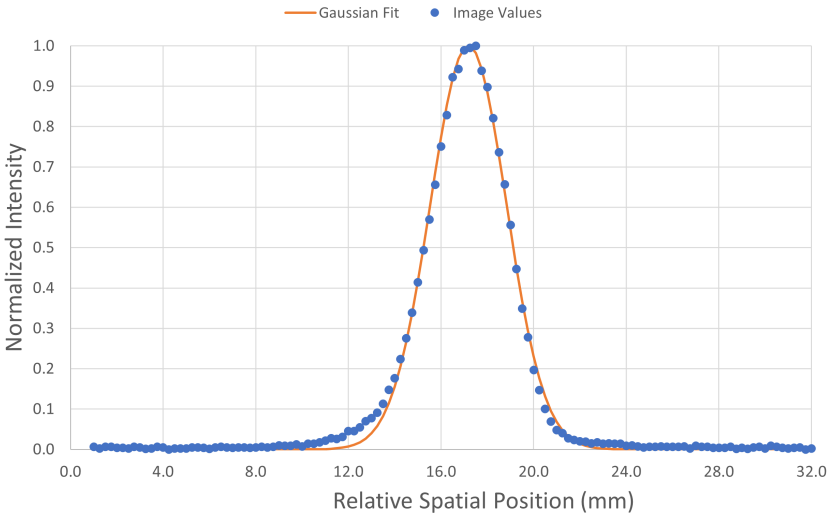

Fig. 12: Line profile of the collimated Cs-137 image on the full radiography panel.

Figure 17 shows the uncorrected and corrected signal-weighted line images. The thinner HDPE blocks used to generate the line decrease the contrast of the line compared to the rest of the image significantly. Because of this, the line is nearly impossible to see in the uncorrected image and just barely visible in the corrected one. Additionally, the lower number of counts caused by a decrease in acquisition time makes the data significantly more noisy, further complicating the MTF measurement. The line was rotated 10° in ImageJ, and an average profile of the line was generated. Both the averaged line values from ImageJ and a fitted Gaussian function to the values are shown in Figure 18. The extremely high amount of noise in the image and the lack of a true zero value where the HDPE blocks covered the panel meant that a Gaussian curve did not fit well to the experimental data. Though the results of an MTF measurement performed on this Gaussian curve may not be high-quality, it was still generated in case it offered any insight into the radiography panel; if the MTF showed promise, a second line measurement could be taken. Figure 19 shows a 90% spatial resolution of approximately 0.30 line pairs per centimeter and a 10% spatial resolution of approximately 1.46 line pairs per centimeter. While these values are a slightly better than the collimated edge results, the high variance and poor Gaussian fit means that these values cannot be trusted as a true improvement in spatial resolution.

Figure 20 shows the uncorrected and corrected signal-weighted line images. Much like the first edge image, the corrected radiograph is much more clear than the uncorrected radiograph, allowing for an accurate MTF measurement to be taken. The edge was rotated 10° in ImageJ, and an average profile of the

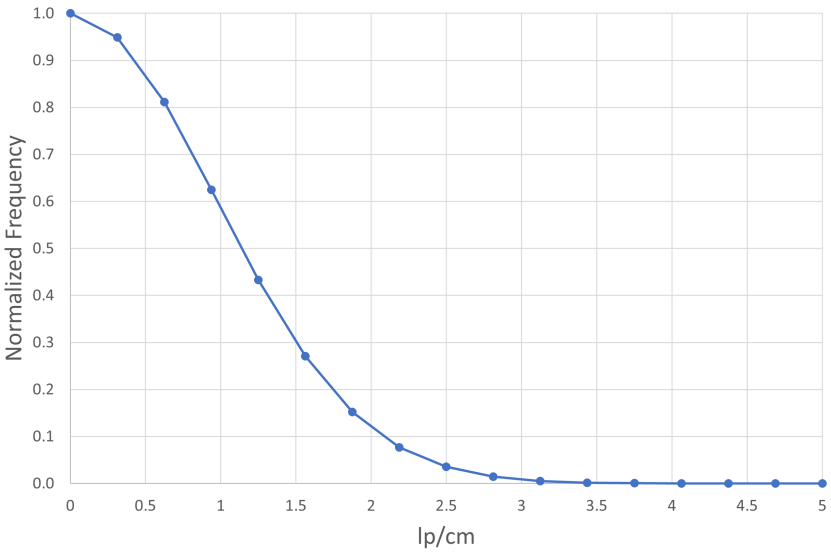

Fig. 13: Modulation transfer function of the collimated Cs-137 line on the full radiography panel.

line was generated. Both the averaged line values from ImageJ and a fitted ERF function to the values are shown in Figure 21. While there are fewer counts in this image compared to the first collimated edge, the variation is still lower than the variation in the edge profile in Young et al. [7]. Figure 22 shows a 90% spatial resolution of approximately 0.27 line pairs per centimeter and a 10% spatial resolution of approximately 1.40 line pairs per centimeter. Both values are slight improvements compared to the first edge measurement. However, this and the other two full-panel MTF measurements are similarly far off from the measurements done on a single ROSSPAD, indicating that the loss in spatial resolution is not the result of a change in experimental setup but rather a change somewhere in the detector configuration or image generation process.

3.3 Comparison to Single-ROSSPAD Images

Table 1 compares the spatial resolution of the different radiography systems for both gamma rays and neutrons, with single-ROSSPAD data taken from Young et al. [7]. For gamma rays, the differences between the single-ROSSPAD system and the multi-ROSSPAD system are relatively minor. The 90% MTF was reduced by 10.6% and the 10% MTF reduced by 9.9%. The decrease in spatial resolution is likely the result in the change of the geometry of the setup for the experiment. With the single ROSSPAD detector, the tungsten blocks could be placed against the face of the scintillator with only tape between them. The full panel, however, has a gap between the scintillator face and

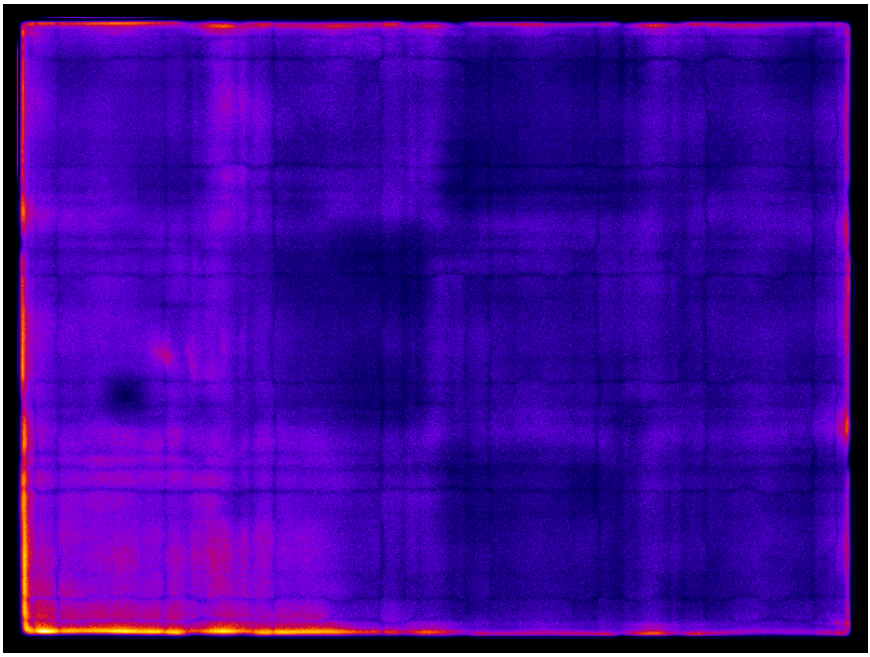

(a) Uncorrected

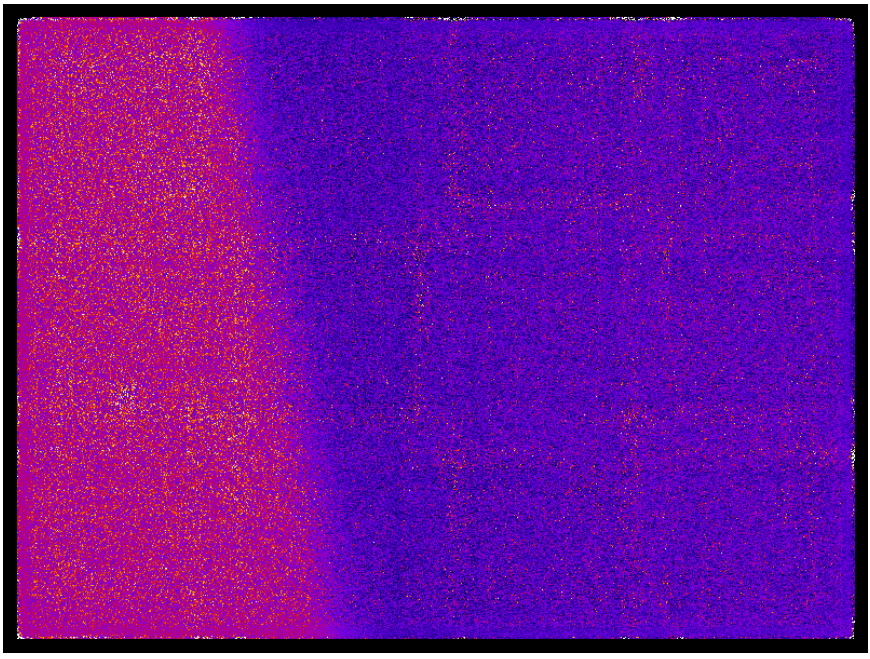

(b) Corrected

Fig. 14: Full-panel Cf-252 collimated edge images that are a) before flood field correction and b) after flood field correction. ($N = 4.70 \times 10^7$ counts)

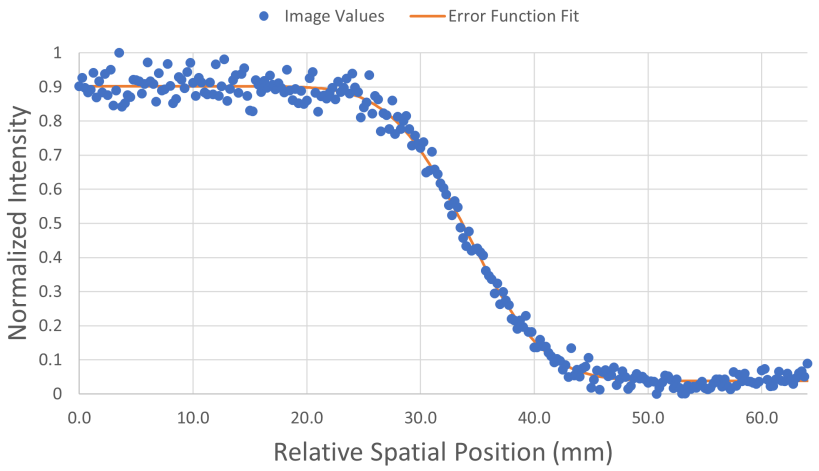

Fig. 15: Line profile of the first collimated Cf-252 edge on the full radiography panel.

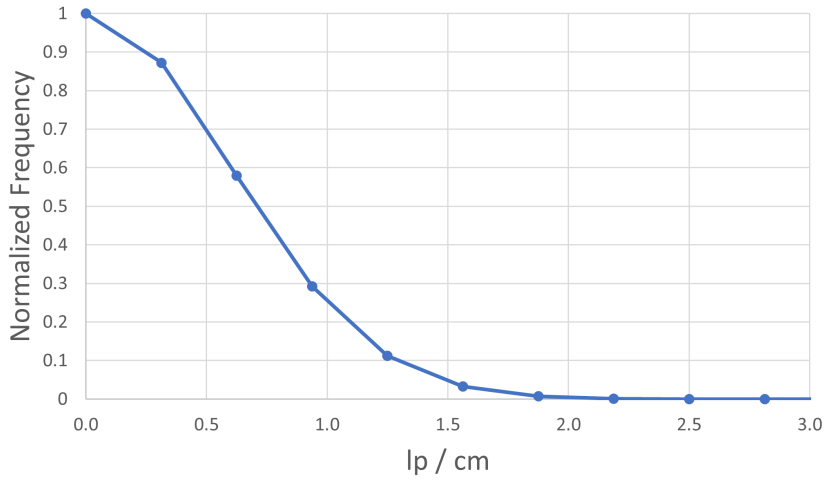

Fig. 16: Modulation transfer function of the first collimated Cf-252 edge on the full radiography panel.

the outside of the housing. Increasing the distance between the object and the detector panel is known to decrease spatial resolution, making detector configuration changes the most-likely culprit for resolution changes [16].

When moving to neutron radiographs, the changes between setups were much more drastic. The three experiments saw decreases in spatial resolution at 90% MTF of 65.7%, 57.1%, and 61.4% respectively. The 90% MTF values

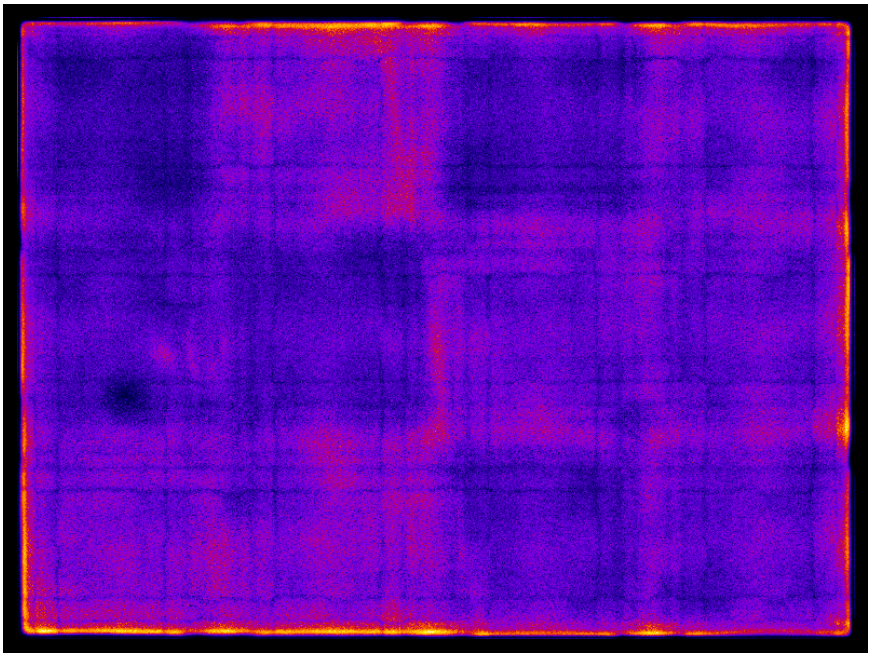

(a) Uncorrected

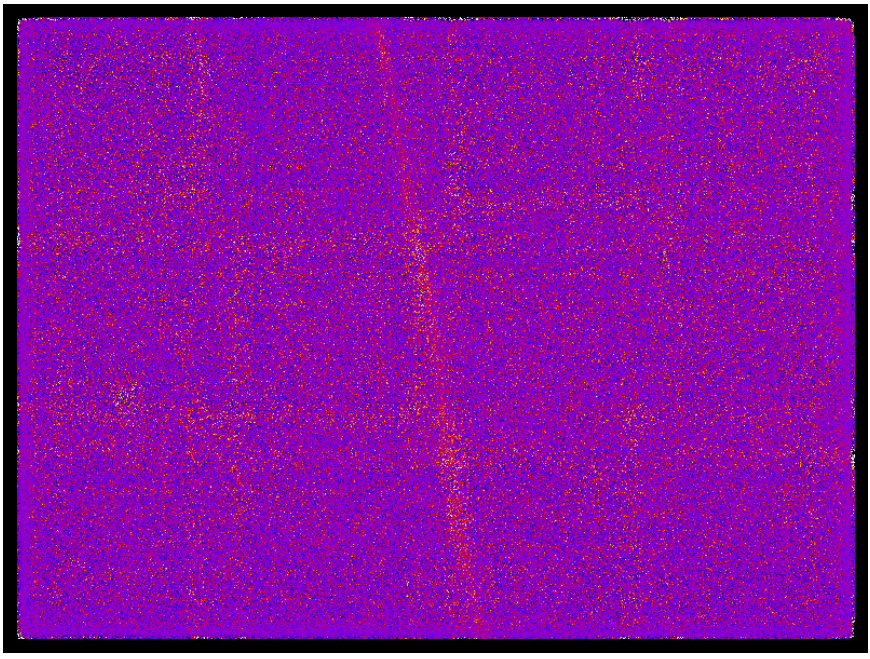

(b) Corrected

Fig. 17: Full-panel Cf-252 collimated line images that are a) before flood field correction and b) after flood field correction. (N = 1.92×10^7 counts)

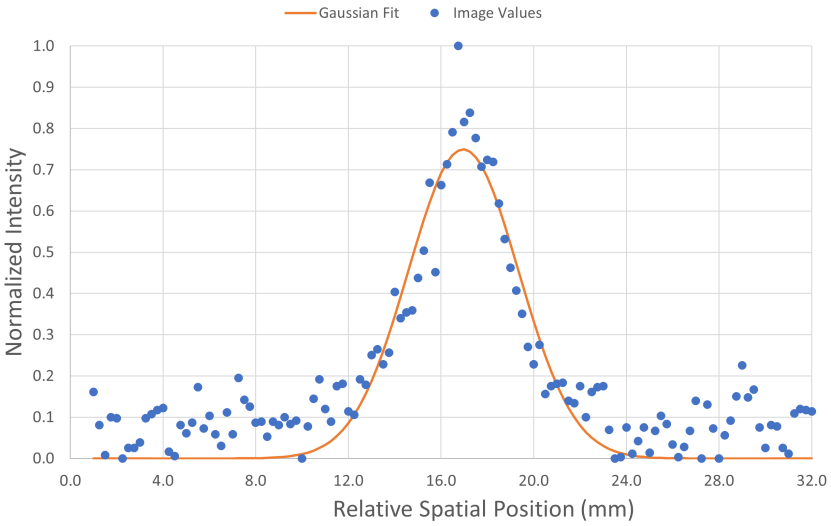

Fig. 18: Profile of the collimated Cf-252 line on the full radiography panel.

saw decreases of 61.2%, 56.4%, and 58.2%. These reductions are significantly higher than the reductions between the Cs-137 MTFs, despite the detector geometry being consistent between the Cs-137 images and the Cf-252 images. Additionally, changes to the experimental setup across the three Cf-252 full-panel MTF measurements demonstrate that the large decrease compared to Cs-137 images is likely connected to the type of radiation used (neutrons vs. gamma rays).

The most likely explanation behind the sudden decrease in spatial resolution is the introduction of more material in front of the ROSSPAD. The full-panel system has an aluminum lid that is a quarter of an inch thick, and compressible foam was added between the lid and the scintillator package to help keep the scintillator in place. The introduction of these materials likely leads to increased scattering for both gammas and neutrons. Gamma rays, after scattering, are more likely to be absorbed at their decreased energies within the aluminum or foam compared to fission spectrum neutrons. The difference between the energies of the two particles (0.662 MeV gammas vs. 2.105 MeV (average) neutrons) and the differences in interaction mechanisms means that the neutron images will be more blurry due to scattering than gamma images will be. Further testing on small-area, multi-ROSSPAD panels with and without the aluminum and foam are needed to further determine if this is the main cause of the decrease in spatial resolution.

3.4 Demonstration Image

Since a Cf-252 fission neutron source was used to generate neutron images, it is important to demonstrate that radiographs with the source are actually

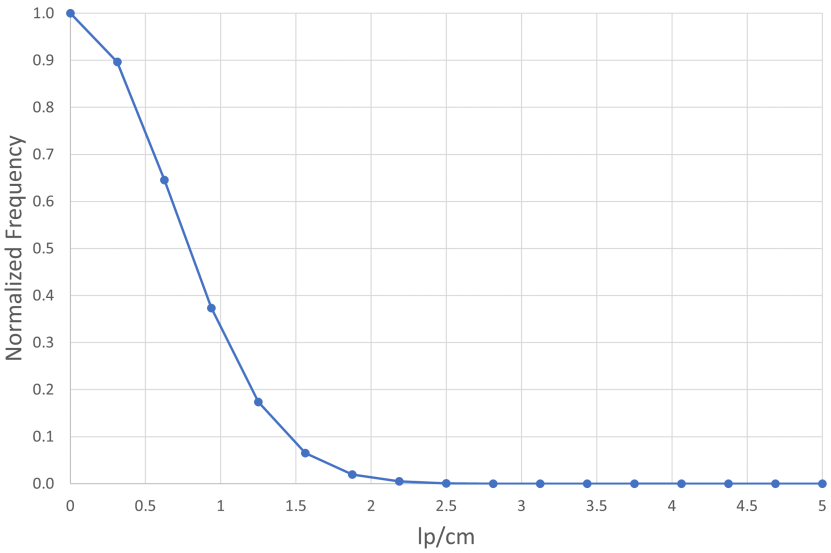

Fig. 19: Modulation transfer function of the collimated Cf-252 line on the full radiography panel.

Table 1: Comparison of Spatial Resolutions

Measurement Setup	90% MTF (lp/cm)	10% MTF (lp/cm)
Cs-137 Line (Single ROSSPAD)	0.47	2.32
Cs-137 Line (Multi-ROSSPAD)	0.42	2.09
Cf-252 Edge (Single ROSSPAD)	0.70	3.35
Cf-252 Edge #1 (Multi-ROSSPAD)	0.24	1.30
Cf-252 Line (Multi-ROSSPAD)	0.30	1.46
Cf-252 Edge #2 (Multi-ROSSPAD)	0.27	1.40

comprised of neutrons and not mostly comprised of gamma rays from daughter products of the Cf-252 isotope. Normally, pulse-shape discrimination (PSD) would help in eliminating many of the gamma rays from the Cf-252 source. However, since the ROSSPAD detectors cannot perform PSD, a new method was developed as a quick test to determine if neutrons are present.

The ratio of the gamma rays that can transmit through an object is governed by the equation:

$$\frac{I}{I_0} = \exp\left(-\frac{\mu}{\rho} * \rho * x\right) \tag{2}$$

where $\frac{I}{I_0}$ is the fraction of the gammas that do not interact with the object, $\frac{\mu}{\rho}$ is the attenuation coefficient of the material, ρ is the density of the object, and x is the thickness of the object. Correction using the flood field gives an

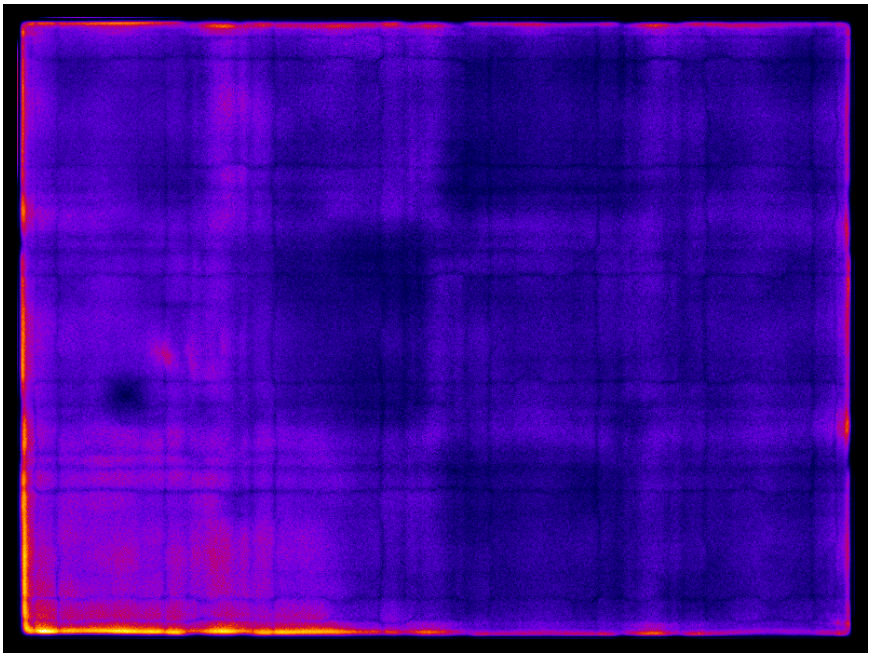

(a) Uncorrected

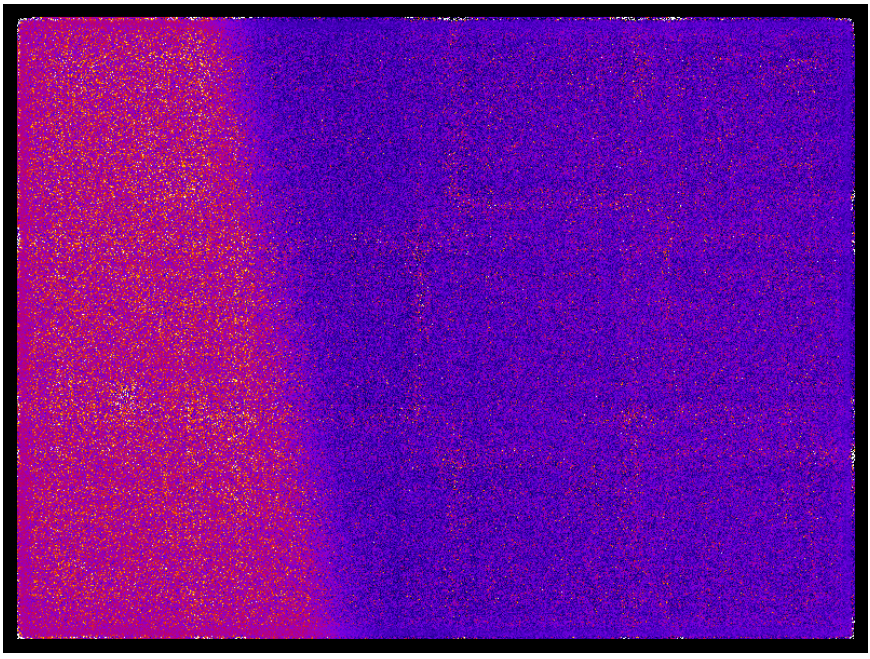

(b) Corrected

Fig. 20: Second full-panel Cf-252 collimated edge images that are a) before flood field correction and b) after flood field correction. ($N = 1.23 \times 10^7$ counts)

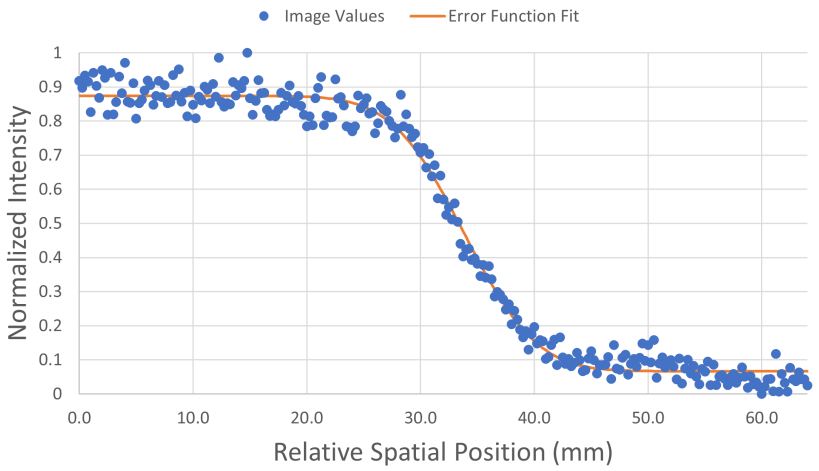

Fig. 21: Line profile of the second collimated Cf-252 edge on the full radiography panel.

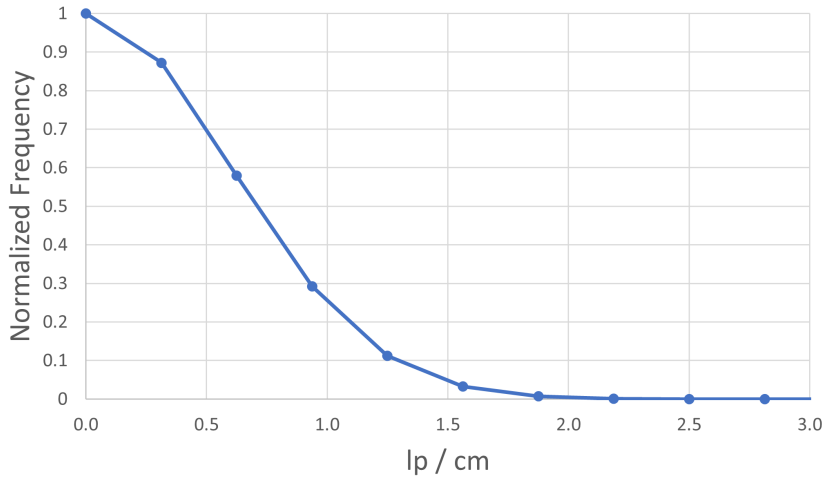

Fig. 22: Modulation transfer function of the second collimated Cf-252 edge on the full radiography panel.

approximation of $\frac{I}{I_0}$, and by rearranging Equation 2 into:

$$\frac{\mu}{\rho} = -\frac{\ln \frac{I}{I_0}}{\rho * x} \tag{3}$$

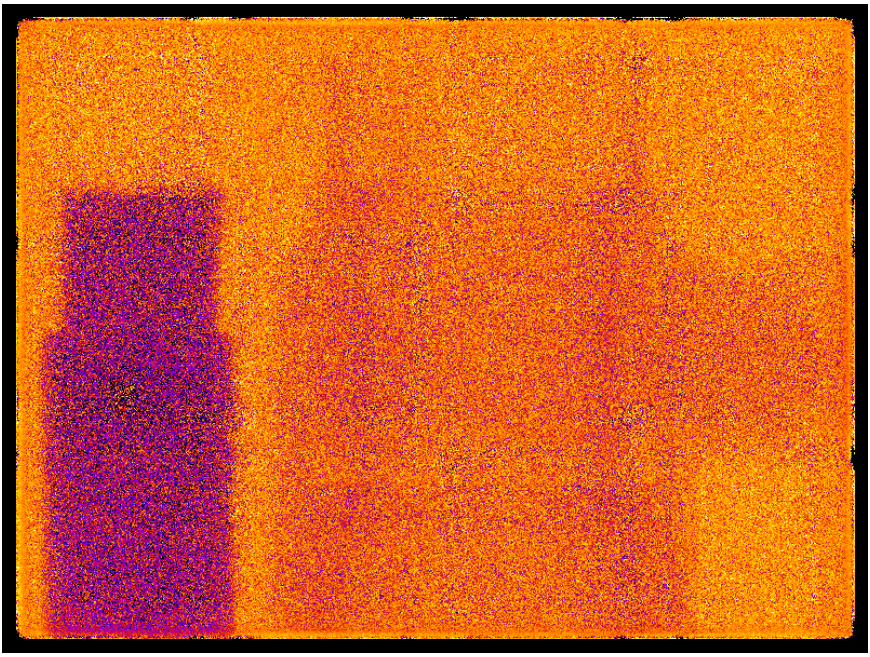

Fig. 23: The resultant neutron radiograph of the tungsten block and the plastic valve.

the approximate transmission coefficient for the incident particles in the material can be derived and compared to NIST XCOM [13].

The resultant radiograph generated using a Cf-252 source is shown in Figure 23. Using ImageJ, the log of the ratio of the image to the flood field is calculated for a large portion of the tungsten block, shown in Figure 24 [12]. By plugging the mean value from ImageJ into Equation 3, as well as the density of tungsten ($19.28 \frac{g}{cm^3}$) and the thickness of the tungsten block ($3.81cm$), an approximate value for the attenuation coefficient of the particles through the tungsten is found to be $1.572 \times 10^{-2} \frac{cm^2}{g}$. In comparison, XCOM lists the total attenuation coefficient of 0.662 MeV gamma rays (from Cs-137) through tungsten to be $9.793 \times 10^{-2} \frac{cm^2}{g}$. These numbers indicate that the particles from the Cf-252 neutron source are approximately 6.2 times more penetrating than the gammas from a Cs-137 source, an indication that the majority of the events in the image come from neutrons and not from gamma rays.

4 Conclusion

A full-panel fast neutron radiography system was built using the IDEAS ROSSPADs. Some simple modifications were needed to convert the single-ROSSPAD imaging processes into full-panel imaging processes. A new aluminum housing was constructed to house a full 6 by 6 ROSSPAD panel, though technical issues

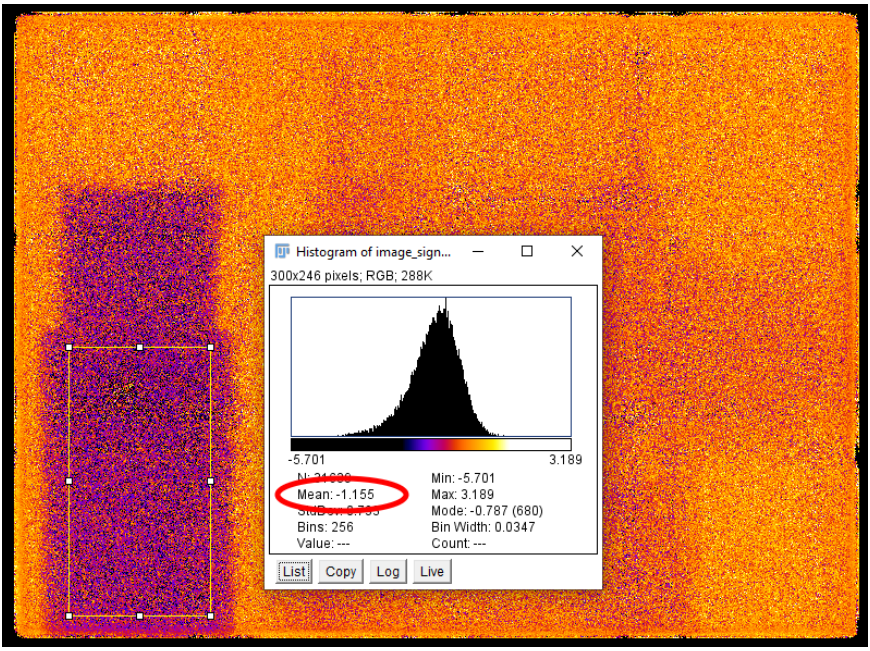

Fig. 24: Mean value of the log of the ratio of the image and the flood field, circled in red. Value generated with ImageJ.

limited the panel to a 4 by 3 usable ROSSPAD area. Changes to gain correction and triggering threshold were needed to appropriately localize events across multiple ROSSPADs. Cs-137 spatial resolution saw a slight reduction from 2.32 line pairs per centimeter at 10% MTF for the single ROSSPAD to 2.09 line pairs per centimeter at 10% MTF for the full panel. Neutron radiographs saw a significant loss in spatial resolution. On a single ROSSPAD, the spatial resolution was 3.35 line pairs per centimeter at 10% MTF. The full panel ranged from 1.46 line pairs per centimeter to 1.30 line pairs per centimeter at 10% MTF. While the example radiograph using a tungsten block and a plastic valve showed promise, the loss of spatial resolution in the panel is a serious concern that needs further exploration before the panel can be used as a regular instrument.

Declarations

Disclaimer

This work of authorship and those incorporated herein were prepared by Consolidated Nuclear Security, LLC (CNS) as accounts of work sponsored by an agency of the United States Government under Contract DE-NA-0001942. Neither the United States Government nor any agency thereof, nor CNS, nor any of their employees, makes any warranty, express or implied, or assumes any

legal liability or responsibility to any non-governmental recipient hereof for the accuracy, completeness, use made, or usefulness of any information, apparatus, product, or process disclosed, or represents that its use would not infringe privately owned rights. Reference herein to any specific commercial product, process, or service by trade name, trademark, manufacturer, or otherwise, does not necessarily constitute or imply its endorsement, recommendation, or favoring by the United States Government or any agency or contractor thereof, or by CNS. The views and opinions of authors expressed herein do not necessarily state or reflect those of the United States Government or any agency or contractor (other than the authors) thereof.

Copyright Notice

Author Contributions

Author C. Young curated the data, performed the analysis, and wrote and edited the manuscript. C. Browning, R. Thurber, and M. Smalley assisted in data curation and analysis under the supervision of C. Young. M. Liesenfelt, J. Hayward, and N. McFarlane supervised the project. J. Preston and M. Cooper provided funding and project administration. All authors reviewed and approved the release of the manuscript.

Funding

This material is based upon work supported by the Department of Energy National Nuclear Security Administration through the Nuclear Science and Security Consortium under Award Number DE-NA0003180.

Availability of Data and Material

Not applicable.

Competing interests

We declare that the authors have no competing interests as defined by Springer, or other interests that might be perceived to influence the results and/or discussion reported in this paper.

Ethical Approval

We have read and understood your journal's ethics, and we believe that neither the manuscript nor the study violates any of these.

Consent for Publication

We have read and understood the publishing policy, and submit this manuscript in accordance with this policy. The results/data/figures in this manuscript have not been published elsewhere, nor are they under consideration by another publisher.

References

[1] D.L. Williams, C.M. Brown, D. Tong, A. Sulyman, C.K. Gary, A fast neutron radiography system using a high yield portable dt neutron source. Journal of imaging **6**(12), 128– (2020)

[2] S. Bishnoi, P.S. Sarkar, R.G. Thomas, T. Patel, M. Pal, P.S. Adhikari, A. Sinha, A. Saxena, S.C. Gadkari, Preliminary experimentation of fast neutron radiography with d-t neutron generator at barc. Journal of nondestructive evaluation **38**(1), 1–9 (2018)

[3] S. Wang, C. Cao, W. Yin, Y. Wu, H. Huo, Y. Sun, B. Liu, X. Yang, R. Li, S. Zhu, C. Wu, H. Li, B. Tang, A novel ndt scanning system based on line array fast neutron detector and d-t neutron source. Materials **15**(14) (2022). https://doi.org/10.3390/ma15144946

[4] P.L. Kerr, N. Cherepy, J. Church, G. Guethlein, J. Hall, C. McNamee, S. O'Neal, K. Champley, A. Townsend, M. Sasagawa, A. Hardy, Neutron transmission imaging with a portable d-t neutron generator (2021). https://doi.org/10.2172/1814672. URL https://www.osti.gov/biblio/1814672

[5] S. McConchie, D. Archer, J. Mihalczo, B. Palles, M. Wright, Transportable, low-dose active fast-neutron imaging. Tech. rep., Oak Ridge National Laboratory (2017). URL https://info.ornl.gov/sites/publications/Files/Pub74146.pdf

[6] M. Heath, B. Canion, L. Fabris, I. Garishvili, A. Glenn, J. Hausladen, P. Hausladen, D. Lee, S. McConchie, L. Nakae, J. Newby, R. Wurtz, Development of a portable pixelated fast-neutron imaging panel. IEEE TRANSACTIONS ON NUCLEAR SCIENCE **69**(6) (2022). https://doi.org/10.1109/TNS.2021.3136344. URL https://www.osti.gov/biblio/1884004

[7] C.X. Young, C.A. Browning, R.J. Thurber, M.R. Smalley, M.J. Liesenfelt, J.P. Hayward, N. McFarlane, M.P. Cooper, J.R. Preston, Scalable detector design for a high-resolution fast-neutron radiography panel. Journal

of Nondestructive Evaluation **42**(4), 87 (2023). https://doi.org/10.1007/s10921-023-00999-x. URL https://doi.org/10.1007/s10921-023-00999-x

[8] Rosspad: Sipm readout module for x-ray and gamma-ray spectroscopy and imaging. URL https://ideas.no/products/rosspad/#

[9] 1207 cmos flat panel detector (2022). URL https://www.vareximaging.com/wp-content/uploads/2022/01/1207-CMOS-Medical_PDS_149126-000.pdf

[10] Noctua.at - premium cooling components designed in austria. URL https://noctua.at/en/nf-a4x20-pwm/specification

[11] A.L.C. Kwan, J.A. Seibert, J.M. Boone, An improved method for flat-field correction of flat panel x-ray detector. Medical Physics **33**(2), 391–393 (2006). https://doi.org/https://doi.org/10.1118/1.2163388. URL https://aapm.onlinelibrary.wiley.com/doi/abs/10.1118/1.2163388. https://arxiv.org/abs/https://aapm.onlinelibrary.wiley.com/doi/pdf/10.1118/1.2163388

[12] Imagej: Image processing and analysis in java. URL https://imagej.net/ij/index.html

[13] M.J. Berger, J.H. Hubbell, Xcom: Photon cross sections on a personal computer. OSTI (1987). https://doi.org/10.2172/6016002

[14] D. Nikezic, M. Beni, D. Krstic, P. Yu, Characteristics of protons exiting from a polyethylene converter irradiated by neutrons with energies between 1 kev and 10 mev. PLOS ONE **11**, e0157,627 (2016). https://doi.org/10.1371/journal.pone.0157627

[15] General Purpose Plastic Scintillator EJ-200, EJ-204, EJ-208, EJ-212 (2023)

[16] R. YASUDA, T. NOJIMA, H. IIKURA, T. SAKAI, M. MATSUBAYASHI, Development of a small-aperture slit system for a high collimator ratio at the thermal neutron radiography facility in jrr-3. Journal of Nuclear Science and Technology **48**(7), 1094–1101 (2011). https://doi.org/10.1080/18811248.2011.9711794. URL https://www.tandfonline.com/doi/abs/10.1080/18811248.2011.9711794. https://arxiv.org/abs/https://www.tandfonline.com/doi/pdf/10.1080/18811248.2011.9711794